Hund's Rule-Driven Dzyaloshinskii-Moriya Interaction at 3d-5d Interfaces

A. Belabbes,[1,*] G. Bihlmayer,[2] F. Bechstedt,[3] S. Blügel,[2] and A. Manchon[1,†]

[1]*King Abdullah University of Science and Technology (KAUST), Physical Science
and Engineering Division (PSE), Thuwal 23955-6900, Saudi Arabia*
[2]*Peter Grünberg Institut and Institute for Advanced Simulation, Forschungszentrum Jülich and JARA, D-52425 Jülich, Germany*
[3]*Institut für Festkörpertheorie und -optik, Friedrich-Schiller-Universität Jena, Max-Wien-Platz 1, 07743 Jena, Germany*

Using relativistic first-principles calculations, we show that the chemical trend of the Dzyaloshinskii-Moriya interaction (DMI) in 3d-5d ultrathin films follows Hund's first rule with a tendency similar to their magnetic moments in either the unsupported 3d monolayers or 3d-5d interfaces. We demonstrate that, besides the spin-orbit coupling (SOC) effect in inversion asymmetric noncollinear magnetic systems, the driving force is the 3d orbital occupations and their spin-flip mixing processes with the spin-orbit active 5d states control directly the sign and magnitude of the DMI. The magnetic chirality changes are discussed in the light of the interplay between SOC, Hund's first rule, and the crystal-field splitting of d orbitals.

Introduction.—Chiral objects are ubiquitous in science [1] and pose fundamental challenges such as the importance of chiral molecules in commercial drugs [2] or the dominance of matter over antimatter in the universe. Magnetic materials lacking inversion symmetry can host chiral magnets and present a unique platform for the exploration and control of chiral objects. The dynamic development of this field has been recently illustrated by the observation of the magnon Hall effect [3,4] or the achievement of room temperature magnetic Skyrmions [5–8], opening avenues for robust high density data storage [9].

A crucial ingredient for the generation of such chiral textures is the Dzyaloshinskii-Moriya antisymmetric magnetic interaction (DMI) [10,11] arising from spin-orbit coupling (SOC) in inversion asymmetric magnets. Originally proposed in the context of Mott insulators [11], weak metallic ferromagnets, and spin glasses [12], major attention has been recently drawn toward the nature of the DMI at transition-metal (TM) interfaces. Such interfaces, consisting of a stack of 3d/5d(4d) transition metals, have been intensively investigated from the viewpoint of mainstream spintronics, resulting in the recent development of spin-orbit torques [13,14] and domain wall-based devices [15]. In these systems, the interfacial DMI gives rise to several exotic magnetic phases such as Néel domain walls [16,17], spin spirals [18], and Skyrmions with a defined chirality [5–7,19].

The ability to understand and control the sign and strength of the DMI remains the big challenge of research in magnetism and may open new approaches to future nanoscale magnetic devices [20]. It demands a qualitative description of the physics of the DMI that can serve as a guideline for materials and interface design. While such models are available in the context of Mott insulators [11], spin glasses [12], and magnetic Rashba gases [21], such a

phenomenology is still lacking for transition-metal interfaces. In fact, the high complexity of interfacial hybridization hinders the development of qualitative and quantitative predictions in these material combinations. Only a few isolated examples have been investigated from first principles [19,22–31]. It is therefore crucial to apply such studies and examine the trends of the DMI across 3d/5d transition metal interfaces, in order to identify the underlying physical mechanisms and develop a predictive physical picture.

In this Letter, we present the first systematic and comprehensive theoretical analysis of the DMI for a large series of 3d transition metals (V, Cr, Mn, Fe, Co, Ni) as overlayers on 5d TM (W, Re, Os, Ir, Pt, Au) substrates. We demonstrate that the sign and magnitude of the DMI are directly correlated to the degree of 3d-5d orbital hybridization around the Fermi energy, which can be controlled by the intra-atomic Hund's exchange field of the 3d overlayer [32,33].

First-principles method.—In order to understand the behavior of the DMI in 3d-5d ultrathin films we have performed density functional theory calculations in the local density approximation [34] to the exchange correlation functional, using the full potential linearized augmented plane wave method in film geometry [35] as implemented in the Jülich density functional theory code FLEUR [36]. Both collinear and noncollinear magnetic configurations have been studied employing an asymmetric film consisting of six substrate layers of 5d TM covered by a pseudomorphic 3d TM monolayer on one side of the film at the distance optimized for the energetically lowest collinear magnetic state. For the noncollinear calculations we used a $p(1 \times 1)$ unit cell applying the generalized Bloch theorem [37]. We considered 512 and 1024 $\mathbf{k}_{\parallel}$ points in the two-dimensional Brillouin zone for calculations including the scalar-relativistic effects and SOC treated within

first-order perturbation theory, respectively [19,22–25, 28–30]. More details on the computation of the spin-spiral and DMI contribution are given in the Supplemental Material [38].

Magnetism of 3d/5d interfaces.—In Fig. 1(a) we display the variation of the magnetic moment across the $3d/5d$ interfaces for their magnetic ground state at equilibrium interlayer distances. A major trend appears: the Mn overlayer has the highest magnetic moment, regardless of the substrate, and it gradually decreases for chemical elements on both sides of Mn in the $3d$ TM row of the periodic table. The magnetic moment, although reduced by about $(1\mu_B–3\mu_B)$, qualitatively follows the total spin S of the $3d$ shell. This trend reveals that the intra-atomic exchange is controlled by the atomiclike nature of the orbitals according to Hund's first rule [32,42,43]. We note that the local magnetic moment of the $3d/5d$ films (solid lines) is reduced with respect to the magnetic moment of the (ideal) unsupported monoatomic $3d$ layers (UML, dashed line). This is a consequence of the increased bonding at the interface due to the orbital hybridization of surface and overlayer states [see Fig. 1(a)].

Figure 1(b) shows that the substrate exhibits an induced spin polarization since the increased bonding with the $3d$ overlayer enhances the magnetic moment of the neighboring $5d$ atoms at the interface. From this figure we conclude that W, Pt, and to some extent Ir are highly polarizable substrates, while the other substrates considered show a relatively small induced magnetic moment at the interface. The induced magnetic moment for Pt and W substrates couples ferromagnetically and antiferromagnetically with the $3d$ overlayer, respectively. Their strong local-spin polarizability is mainly due to the high spin susceptibility
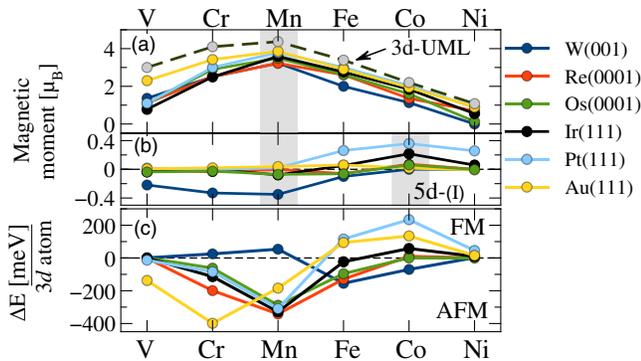
originating from the large Stoner exchange parameter. For the Au substrate, on the other hand, there is almost no or only very weak polarization since the $3d$ orbitals do not hybridize with the energetically low-lying $5d$ states of Au.

To complete the description of the transition-metal interfaces, we analyze the magnetic stability of $3d$ overlayers on various $5d$ substrates in terms of the total energy difference $\Delta E = E_{\mathrm{AFM}} - E_{\mathrm{FM}}$ as shown in Fig. 1(c). We primarily focus on three collinear configurations: the ferromagnetic (FM) state, the row-wise $p(1 \times 2)$-antiferromagnetic (AFM) state for (111) and (0001) surfaces, and the checkerboard $c(2 \times 2)$-AFM states for (001)-oriented surfaces (see Fig. 1 in the Supplemental Material [38]). For a W(001) substrate, we clearly observe the opposite trend for the early $3d$ overlayer elements V, Cr, and Mn compared to all other considered $5d$ substrates, in good agreement with the theoretical study by Ferriani *et al.* [43], who predicted the same energetic ordering for $3d$/W(001). We find that the magnetic ground state is AFM for all substrates, while it is FM for W with small energy differences between the two magnetic configurations. In the case of Mn/W(001) the row-wise $p(1 \times 2)$-AFM state is energetically more favorable than the checkerboard $c(2 \times 2)$-AFM configuration by ~ 0.3 eV/Mn atom. However, for Ni, Co, and Fe, moving from right to left through the $5d$ elements, we observe a strong tendency from FM ordering toward an AFM coupling as a function of the $5d$ band filling of the substrate.

We notice that the $3d$-$5d$ interface states around the Fermi energy and their relative lineup control the competition between FM and AFM coupling of the deposited $3d$ atoms [43,45,46]. This especially holds when the nearest-neighbor exchange interaction $\Delta E = E_{\mathrm{AFM}} - E_{\mathrm{FM}}$ is small as shown in Fig. 1(c). In this case, complex magnetic textures can be expected in the presence of SOC since the antisymmetric exchange Dzyaloshinskii-Moriya interaction [10,11] contributes considerably to the total energy. Indeed, if it is sufficiently strong to compete with the magnetocrystalline anisotropy and the Heisenberg exchange, it can stabilize long-range chiral magnetic order such as Skyrmions or homochiral spin spirals [18,19].

Dzyaloshinskii-Moriya interaction.—Phenomenologically, the DMI has the typical form $E_{\mathrm{DM}} = \sum_{i,j} \mathbf{D}_{ij} \cdot (\mathbf{S}_i \times \mathbf{S}_j)$, where $\mathbf{D}_{ij}$ determines the strength and sign of the DMI, and $\mathbf{S}_i$ and $\mathbf{S}_j$ are magnetic spin moments located on neighboring atomic sites i and j (see the Supplemental Material for more details [38]). The energy contribution to the DMI due to SOC treated in first order perturbation theory [25,37,39–41,47] corresponds to the sum of all energy shifts from filled states, $E_{\mathrm{DMI}}(\mathbf{q}) = \sum_{\mathbf{k}\nu}^{\mathrm{occ}} n_{\mathbf{k}\nu}(\mathbf{q})\delta\epsilon_{\mathbf{k}\nu}(\mathbf{q})$, with $n_{\mathbf{k}\nu}(\mathbf{q})$ the occupation numbers of state $|\psi_{\mathbf{k}\nu}(\mathbf{q})\rangle$ (ν-band index, $\mathbf{k}$-Bloch vector) and $\mathbf{q}$ the wave-vector propagation of the spin spiral. Here, the energy shift of the occupied states with respect to the scalar-relativistic (SR) calculation corresponds

FIG. 1. (a) Calculated magnetic moments of the $3d$ TM monolayers on $5d$ substrates compared to the moments of the $3d$ UML indicated by the dashed black line. (b) The magnetic moments of interface $5d$ atoms [44]. (c) The magnetic order of $3d$ monolayers on $5d$ substrates using different configurations: the FM, row-wise $p(1 \times 2)$-AFM, and checkerboard $c(2 \times 2)$-AFM states for the square lattice (001); the FM and AFM states for the (111) and (0001) oriented surfaces. A positive $\Delta E = E_{\mathrm{AFM}} - E_{\mathrm{FM}}$ indicates a FM ground state, while negative values denote an AFM order.

to $\delta\epsilon_{\mathbf{k}\nu} = \epsilon_{\mathbf{k}\nu}^{\mathrm{SOC}} - \epsilon_{\mathbf{k}\nu}^{\mathrm{SR}}$. In the limit of smooth magnetic textures ($q \to 0$), the DMI can be directly determined by a linear fit, $E_{\mathrm{DMI}}(\mathbf{q}) \approx Dq$ [39]. In order to further understand the layer-resolved DMI energy $E_{\mathrm{DMI}}^{\mu}(\mathbf{q})$ (μ labels the atom in the unit cell), we consider the site decomposition of the SOC operator $\mathcal{H}_{\mathrm{so}} = \Sigma_{\mu}\xi(r^{\mu})\sigma L^{\mu}$, where ξ is the SOC strength related to the spherical muffin-tin potential $V(r^{\mu})$, $\xi \sim r^{-1}dV/dr$, $\mathbf{r}^{\mu} = \mathbf{r} - \mathbf{R}^{\mu}$, and $|\mathbf{r}^{\mu}| < R_{\mathrm{MT}}^{\mu}$. $\mathbf{R}^{\mu}$ references the center and R_{MT}^{μ} is the radius of the μth muffin-tin sphere, and μ runs over all atoms in the unit cell.

The central result of this Letter is summarized in Fig. 2(a) (see also Tables I and II in Ref. [38]). There, the total DMI energy D^{tot} is represented as a function of the 3d overlayer element for various 5d substrates. Apart from 3d/Au(111) interfaces, the calculations reveal a very surprising trend in which the modulus of the D vector, i.e., the DMI energy divided by the square of the spin magnetic moment $M_{3d/5d}^2$, across the 3d/5d interfaces follows Hund's first rule with a tendency similar to their magnetic trends in either the 3d UML or 3d/5d ultrathin films [see Fig. 2(b)]. In low-dimensional systems the spin moments as a function of the number of d electrons are well described by Hund's first rule [32,42,46,48]. For the D vector, such a correlation has been neither experimentally nor theoretically demonstrated for 3d/5d thin films. This fact is surprising as it is opposite to what is expected from the knowledge of magnetism in bulk and thin films, especially given that such a correlation does not hold for the proximity-induced magnetization, Heisenberg exchange parameters J_{ij}, and the magnetic energy anisotropy [20,46,49–51] [see also Figs. 1(a)–1(c) and Fig. 2]. Indeed, the nearest-neighbor exchange interaction (J_1) for 3d TMs follows perfectly the Bethe-Slater curve and not Hund's first rule [51]. More specifically, since the
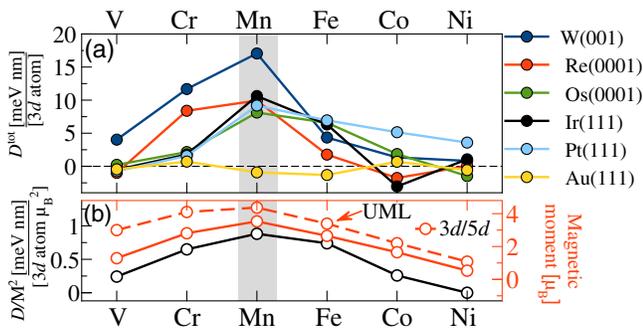
DMI emerges from a complex interplay between (i) the degree of spin polarization of the 3d/5d interface atoms and their band filling, (ii) the strength of SOC in the underlying heavy metal 5d substrate, and (iii) the inversion symmetry breaking at the interface, one does not necessarily expect a direct correlation between the magnetism of the 3d overlayer and the DMI. In the discussion section we will explain in more detail the physical reasons behind the unexpected trend.

In Fig. 2(a) the largest absolute DMI values are obtained for Mn/5d films, regardless of the substrate, with a maximum value of 17 meV nm for Mn/W(001). They monotonically decrease toward V and Ni atoms. In contrast, despite the large SOC of Au, the DMI in 3d/Au almost vanishes due to the completely filled d shell of the Au substrate, irrespective of the 3d overlayer [see Fig. 2(a)]. This remarkable finding demonstrates that the DMI does depend critically not only on SOC and the lack of the inversion symmetry, but also on the d wave function hybridization of the studied 3d/5d interface. The latter affects significantly the interlayer hopping of electrons and, consequently, the magnetic coupling between the 3d overlayer. It is also worthwhile to note that most of the 3d/5d interfaces have a positive sign for the DMI, left or right rotating depending on their magnetic ground state [cf. Fig. 1(c) and Fig. 2] [52].

Discussion.—For the analysis below, it is worth emphasizing that the delocalized 5d wave functions are responsible for the SOC matrix elements $\mathcal{H}_{\mathrm{so}}(\xi L)$ and make essential contributions to the DMI [see Fig. 3(a)]. This behavior is confirmed by the layer-resolved DMI parameter D^{μ} [Fig. 3(b)], which indicates that the sign and strength of the DMI are mainly ascribable to the large contribution of the 5d surface: 80% of the total DMI strength D^{tot} comes from the first two 5d surface layers depending only weakly on the 3d overlayer. An analogous behavior has been identified for the Rashba effect, where 90% of the Rashba splitting is dominated by the 5d surface state wave function [53,54]. However, despite the weak SOC in the 3d overlayer their intra-atomic exchange field can easily modify the electronic structure around the Fermi energy and consequently change the strength of the DMI.
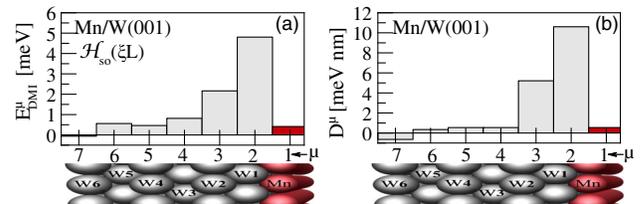

FIG. 2. (a) Strength and sign of the Dzyaloshinskii-Moriya interaction D^{tot} in 3d TM monolayers on 5d substrates calculated around their magnetic ground state combining the relativistic SOC effect with spin spirals. A positive sign of D^{tot} indicates a left-rotational sense or "left chirality". (b) Correlation between $E_{\mathrm{DMI}} \sim D^{\mathrm{tot}}/M_{3d/5d}^2$ averaged over 3d/5d interfaces (black line) versus the adlayer, the magnetic moments in the 3d TM UML (dashed red line), and the local magnetic moment per atom averaged over 3d/5d interfaces (solid red line).

FIG. 3. (a) Layer-resolved $E_{\mathrm{DMI}}^{\mu}(\mathbf{q})$ of the long-period lengths for Mn/W(001) and (b) the DMI strength D^{μ} extracted through a linear fit [$E_{\mathrm{DMI}}^{\mu}(\mathbf{q}) \approx D^{\mu}q$]. Note that the positive sign of D^{tot} ($D^{\mathrm{tot}} = \Sigma_{\mu}D^{\mu}$) indicates left chirality.

The results displayed in Figs. 1 and 2 demonstrate a systematic correlation between the DMI and the magnetic moment on the one hand, and the DMI and the energetic positions of the $3d/5d$ states on the other hand. This mechanism can be understood by examining the band alignment of the $3d$ and $5d$ states and their spin-flip mixing processes, since the anisotropic exchange mechanism requires spin-flip transitions between occupied and unoccupied states that involve spin-orbit active states [11,25]. Note that the intermediate $5d$ states are necessary for the spin-flip process to unoccupied states of the other spin channel.

The basic idea is illustrated in Fig. 4, where the electronic configurations of the $3d$ orbitals and their spin-split band positions with respect to $5d$ W states are displayed. Since the $5d$ bandwidth is significantly larger than the crystal-field splitting and the $5d$ states are weakly polarized (degenerate and partially filled), the overall physics is mostly governed by the band lineup of $3d$ spin channels, themselves determined by Hund's first rule. According to this rule, for the V and Ni overlayers both spin channels are almost occupied or unoccupied and consequently transitions between these states do not contribute anymore to the DMI. We emphasize that occupied and unoccupied states should be available for the $3d$ electrons to allow for spin-flip excitations. In the case of Co, some spin-down states become unoccupied and transitions into these states contribute only weakly to the DMI. Hence, depending on the substrate states, the DMI
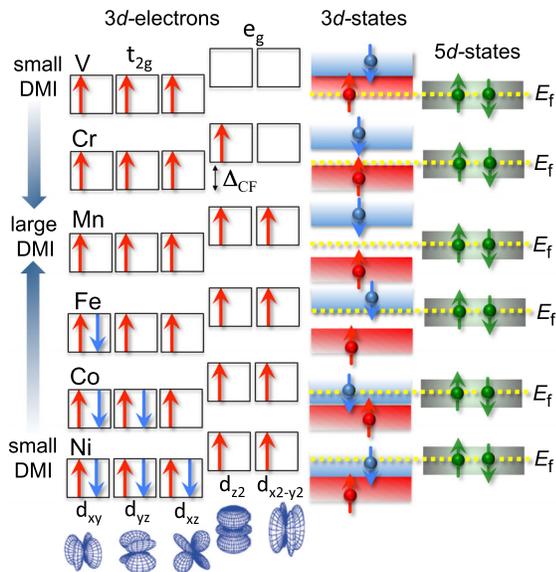

FIG. 4. Left: filling with electrons of $3d$ TM elements into the five $3d$ orbitals according to Hund's first rule; spin-up and spin-down are shown by red and blue arrows, respectively. On the right side we show the spin-split band positions of $3d$ states with respect to $5d$ W states. Note, since the $5d$ bandwidth is significantly larger than the crystal-field splitting the $5d$ states are degenerate at the Fermi level. Δ_{CF} indicates the crystal-field splitting between the t_{2g} and e_g shells.

can exhibit an oscillation in sign (i.e., left- or right-hand chirality) as shown in Fig. 2. This also holds true for Ni/$5d$ and V/$5d$ interfaces on both sides of this trend. However, in the case of Mn the filling of the five Mn $3d$ orbitals adopts a stable "high spin state" due to the small crystal-field splitting between the t_{2g} and e_g shells [see Fig. 4]. As a result, the spin-up (spin-down) channels are entirely occupied (unoccupied) and all transitions contribute to the DMI through the intermediate spin-orbit active $5d$ states. In other words, the $3d$-$5d$-$3d$ electron hopping is facilitated, resulting in a large DMI [30]. Note that the situation is almost similar for the half-filled Fe and Cr atoms but the exchange splitting is reduced, where most of the Fe spin-down (Cr spin-up) states are still unoccupied (occupied). This fact clearly explains the sensitivity of the DMI to the choice of the $3d$ overlayer and the degree of hybridization with $5d$ states in Fig. 2 (see, e.g., Ref. [43]). Regarding the sign of D in the half-filled $3d$ shells (Fe, Mn, Cr), the DMI prefers to maintain its left-hand chirality (left rotating). Therefore, although some subtleties can be observed when the DMI is small as discussed above, the atomic Hund's first rule overall gives a clear trend of the overlayer dependence of the DMI. Since the electronic configuration of the $5d$ orbitals is governed by either the bandwidth or crystal-field splitting, these scenarios are valid for all $3d/5d$ interfaces, irrespective of the substrate. The latter supports the general physical picture that the DMI at $3d/5d$ interfaces follows the $3d$ orbital occupation and hence Hund's first rule [43]. The Au substrate is an exception since the spin-orbit $5d$ states should dominate at the Fermi level and have to be energetically close to unoccupied minority spin states to facilitate the spin-flip processes necessary for the DMI [55].

Based on the above scenarios, the interplay between Hund's exchange, crystal-field splitting, and SOC should be generally considered in any "design" of the DMI. The band lineup determined by Hund's rule controls not only the $3d$ spin-flip transitions but also their spin-mixing processes with the spin-orbit active $5d$ states [see Figs. 2 and 4]. Summarizing the results for all $3d/5d$ interfaces, we conclude that for an interface with a $3d$ overlayer that has a band gap around the Fermi energy in both spin channels, a rather large DMI energy should be expected. This fact also relates to the gradual decrease of the DMI for chemical elements on both sides of Mn in the $3d$ TM row of the periodic table, although in low-symmetry environments additional factors may play a role [30]. In this context, the atomic Hund's first rule is a powerful guideline to control the sign and magnitude of the DMI in particular since the total energy contribution also involves a proportionality to $M_{3d/5d}^2$.

In summary, we have predicted the systematic trend of the DMI in $3d$-$5d$ ultrathin films using first-principles calculations. In particular, we demonstrated that the sign and strength of the DMI depend strongly on the degree of

hybridization between $3d$-$5d$ states around the Fermi level. Furthermore, in addition to (i) the strength of SOC in the underlying heavy metal $5d$ substrate, (ii) the degree of the inversion symmetry breaking at the interface, and (iii) the $5d$ band filling, we show that the driving force behind the peculiar behavior of the DMI is the $3d/5d$ band lineup controlled by the Hund's rule filling of $3d$ shells, which also plays a decisive role in the general picture of spin dynamics. We anticipate that our prediction will provide guidance for the experimental realization and further investigation of chiral properties of ultrathin magnetic films.

---

[*]abderrezak.belabbes@kaust.edu.sa

[†]aurelien.manchon@kaust.edu.sa

[1] R. A. Hegstrom and D. K. Kondepudi, Sci. Am. **262**, 108 (1990).

[2] A. R. Maureen, Chemical and Engineering News **82**, 47 (2004).

[3] Y. Onose, T. Ideue, H. Katsura, Y. Shiomi, N. Nagaosa, and Y. Tokura, Science **329**, 297 (2010).

[4] A. Manchon, P. B. Ndiaye, J. H. Moon, H. W. Lee, and K. J. Lee, Phys. Rev. B **90**, 224403 (2014).

[5] C. Moreau-Luchaire et al., Nat. Nanotechnol. **11**, 444 (2016).

[6] O. Boulle et al., Nat. Nanotechnol. **11**, 449 (2016).

[7] W. Jiang et al., Science **349**, 283 (2015).

[8] Y. Tokunaga, X. Z. Yu, J. S. White, H. M. Rønnow, D. Morikawa, Y. Taguchi, and Y. Tokura, Nat. Commun. **6**, 7638 (2015).

[9] A. Fert, V. Cros, and J. Sampaio, Nat. Nanotechnol. **8**, 152 (2013).

[10] I. Dzyaloshinsky, Sov. Phys. JETP **4**, 241 (1958).

[11] T. Moriya, Phys. Rev. **120**, 91 (1960).

[12] A. Fert and P. M. Levy, Phys. Rev. Lett. **44**, 1538 (1980).

[13] I. M. Miron, K. Garello, G. Gaudin, P.-J. Zermatten, M. V. Costache, S. Auffret, S. Bandiera, B. Rodmacq, A. Schuhl, and P. Gambardella, Nature (London) **476**, 189 (2011).

[14] L. Liu, C.-T. Chen, and J. Z. Sun, Nat. Phys. **10**, 561 (2014).

[15] S.-H. Yang, K.-Su Ryu, and S. Parkin, Nat. Nanotechnol. **10**, 221 (2015).

[16] A. Thiaville, S. Rohart, É. Jué, V. Cros, and A. Fert, Europhys. Lett. **100**, 57002 (2012).

[17] K.-Su Ryu, L. Thomas, S.-H. Yang, and S. Parkin, Nat. Nanotechnol. **8**, 527 (2013).

[18] M. Bode, M. Heide, K. von Bergmann, P. Ferriani, S. Heinze, G. Bihlmayer, A. Kubetzka, O. Pietzsch, S. Blügel, and R. Wiesendanger, Nature (London) **447**, 190 (2007).

[19] S. Heinze, K. von Bergmann, M. Menzel, J. Brede, A. Kubetzka, R. Wiesendanger, G. Bihlmayer, and S. Blügel, Nat. Phys. **7**, 713 (2011).

[20] A. Belabbes, G. Bihlmayer, S. Blügel, and A. Manchon, Sci. Rep. **6**, 24634 (2016).

[21] K. W. Kim, H. W. Lee, K. J. Lee, and M. D. Stiles, Phys. Rev. Lett. **111**, 216601 (2013).

[22] P. Ferriani, K. von Bergmann, E. Y. Vedmedenko, S. Heinze, M. Bode, M. Heide, G. Bihlmayer, S. Blügel, and R. Wiesendanger, Phys. Rev. Lett. **101**, 027201 (2008).

[23] M. Menzel, Y. Mokrousov, R. Wieser, J. E. Bickel, E. Vedmedenko, S. Blügel, S. Heinze, K. von Bergmann, A. Kubetzka, and R. Wiesendanger, Phys. Rev. Lett. **108**, 197204 (2012).

[24] Y. Yoshida, S. Schroder, P. Ferriani, D. Serrate, A. Kubetzka, K. von Bergmann, S. Heinze, and R. Wiesendanger, Phys. Rev. Lett. **108**, 087205 (2012).

[25] V. Kashid, T. Schena, B. Zimmermann, Y. Mokrousov, S. Blügel, V. Shah, and H. G. Salunke, Phys. Rev. B **90**, 054412 (2014).

[26] S. Bornemann, O. Šipr, S. Mankovsky, S. Polesya, J. B. Staunton, W. Wurth, H. Ebert, and J. Minár, Phys. Rev. B **86**, 104436 (2012).

[27] E. Simon, K. Palotás, B. Ujfalussy, A. Deák, G. M. Stocks, and L. Szunyogh, J. Phys. Condens. Matter **26**, 186001 (2014).

[28] B. Dupé, M. Hoffmann, C. Paillard, and S. Heinze, Nat. Commun. **5**, 4030 (2014).

[29] B. Zimmermann, M. Heide, G. Bihlmayer, and S. Blügel, Phys. Rev. B **90**, 115427 (2014).

[30] B. Schweflinghaus, B. Zimmermann, M. Heide, G. Bihlmayer, and S. Blügel, Phys. Rev. B **94**, 024403 (2016).

[31] H. Yang, A. Thiaville, S. Rohart, A. Fert, and M. Chshiev, Phys. Rev. Lett. **115**, 267210 (2015).

[32] F. Hund, Z. Phys. **40**, 742 (1927).

[33] A. A. Khajetoorians, M. Valentyuk, M. Steinbrecher, T. Schlenk, A. Shick, J. Kolorenc, A. I. Lichtenstein, T. O. Wehling, R. Wiesendanger, and J. Wiebe, Nat. Nanotechnol. **10**, 958 (2015).

[34] J. P. Perdew and A. Zunger, Phys. Rev. B **23**, 5048 (1981).

[35] E. Wimmer, H. Krakauer, M. Weinert, and A. J. Freeman, Phys. Rev. B **24**, 864 (1981).

[36] http://www.flapw.de.

[37] Ph. Kurz, F. Förster, L. Nordström, G. Bihlmayer, and S. Blügel, Phys. Rev. B **69**, 024415 (2004).

[38] See Supplemental Material at http://link.aps.org/ supplemental/10.1103/PhysRevLett.117.247202, which includes Refs. [37, 39–41], for details of the electronic structure calculations.

[39] M. Heide, G. Bihlmayer, and S. Blugel, Phys. Rev. B **78**, 140403 (2008).

[40] M. Heide, G. Bihlmayer, and S. Blügel, Physica (Amsterdam) **404B**, 2678 (2009).

[41] M. Heide et al., Spin Orbit Driven Physics at Surfaces (Psi-k scientific highlight No. 78, 2006).

[42] S. Blügel, Phys. Rev. Lett. **68**, 851 (1992).

[43] P. Ferriani, S. Heinze, G. Bihlmayer, and S. Blügel, Phys. Rev. B **72**, 024452 (2005).

[44] The AFM order does not show any induced spin polarization at the interface layer for symmetry reasons.

[45] F. Bechstedt, *Principles of Surface Physics* (Springer-Verlag, Berlin, 2003).

[46] S. Blügel and G. Bihlmayer, in *Magnetism of Low-dimensional Systems: Theory*, edited by H. Kronmüller and S. Parkin, Handbook of Magnetism and Advanced Magnetic Materials (John Wiley & Sons, Ltd., Chichester, UK, 2007) pp. 598–640.

[47] The error bars for the SOC energies can be estimated on the order of 0%-20% for perturbations beyond those of first order; for more details see Ref. [40].

[48] L. de Medici, J. Mravlje, and A. Georges, Phys. Rev. Lett. **107**, 256401 (2011).

[49] J. Gayles, F. Freimuth, T. Schena, G. Lani, P. Mavropoulos, R. A. Duine, S. Blügel, J. Sinova, and Y. Mokrousov, Phys. Rev. Lett. **115**, 036602 (2015).

[50] K.-S. Ryu *et al.*, Nat. Commun. **5**, 3910 (2014).

[51] Y. O. Kvashnin, R. Cardias, A. Szilva, I. DiMarco, M. I. Katsnelson, A. I. Lichtenstein, L. Nordström, A. B. Klautau, and O. Eriksson, Phys. Rev. Lett. **116**, 217202 (2016).

[52] For Fe/Ir, Co/Os, Co/Re, Ni/5d, and V/5d interfaces the small energy difference between the FM and the AFM configuration, as shown in Fig. 1(c), is found to be extremely sensitive to the computational details. Accordingly, the magnetic chirality can be on the left or right hand depending on the collinear ground state.

[53] S. Grytsyuk, A. Belabbes, P. M. Haney, H. W. Lee, K. J. Lee, M. D. Stiles, U. Schwingenschlogl, and A. Manchon, Phys. Rev. B **93**, 174421 (2016).

[54] G. Bihlmayer, Y. M. Koroteev, P. M. Echenique, E. V. Chulkov, and S. Blügel, Surf. Sci. **600**, 3888 (2006).

[55] Because the 5d states lie far below the Fermi level, the DMI becomes weaker and shows variations in the sign as a function of the 3d overlayer (Fig. 2, yellow line).